Clinical Translation of Ferumoxytol-Based Vessel Size Imaging (VSI): Feasibility in a Phase I Oncology Clinical Trial Population

Jill Fredrickson[1], **Natalie J. Serkova**[2], **Shelby K. Wyatt**[3], **Richard A. D. Carano**[3], **Andrea Pirzkall**[1], **Ina Rhee**[1], **Lee S. Rosen**[4], **Alberto Bessudo**[5], **Colin Weekes**[6], and **Alex de Crespigny**[1]

[1]Oncology Clinical Development, Genentech, Inc., South San Francisco, CA, USA

[2]Department of Anesthesiology, University of Colorado Cancer Center, Aurora, CO, USA

[3]Department of Biomedical Imaging, Genentech, Inc., South San Francisco, CA, USA

[4]Department of Medicine, Division of Hematology and Oncology, UCLA, Santa Monica, CA, USA

[5]San Diego Pacific Oncology Hematology Associates, Inc., Encinitas, CA, USA

[6]Department of Medical Oncology, University of Colorado Cancer Center, Aurora, CO, USA

Abstract

Purpose—To assess the feasibility of acquiring VSI metrics using ferumoxytol injections and stock pulse sequences in a multi-center Phase I trial of a novel therapy in patients with advanced metastatic disease.

Methods—Scans were acquired before, immediately after, and 48 h after injection, at screening and after 2 weeks of treatment. R_2, R_2*, vessel density (Q), and relative vascular volume fractions (VVF) were estimated in both normal tissue and tumor, and compared to model-derived theoretical and experimental estimates based on preclinical murine data.

Results—Relaxation rates were still significantly elevated in tumors and liver 48 h after ferumoxytol injection; liver values returned to baseline by week 2. Q was relatively insensitive to changes in R_2*, indicating lack of dependence on contrast agent concentration. Variability in Q was higher amongst human tumors compared to xenografts and was mostly driven by R_2. Relative VVFs were higher in human tumors compared to xenografts, while values in muscle were similar between species.

Conclusion—Clinical ferumoxytol-based VSI is feasible using standard MRI techniques in a multi-center study of patients with lesions outside the brain. Ferumoxytol accumulation in the liver does not preclude measurement of VSI parameters in liver metastases.

Keywords

angiogenesis; tumor; vessel size; DCE-MRI; USPIO; VSI

For correspondence please contact: Jill Fredrickson, BioOncology ECD, Genentech, Inc., 1 DNA Way, MS-442A, South San Francisco, CA 94080, fredrickson.jill@gene.com.

Introduction

Quantitative MRI-based techniques are increasingly used in early-phase oncology trials to monitor changes in tumor microvasculature associated with novel anti-angiogenic therapies. Dynamic contrast-enhanced MRI (DCE-MRI), the most common method used to assess anti-angiogenic therapies {O'Connor, 2012 #45}, requires rapid image acquisition during the bolus injection of a gadolinium chelate, providing a mixed measure of tumor perfusion and permeability and relative model-based measures of extravascular extracellular and blood plasma volumes {Tofts, 1999 #48}. DCE-MRI has proven useful for evaluating drugs where the mechanism-of-action includes changes in vascular permeability, such as those targeting vascular endothelial growth factor (VEGF, i.e. bevacizumab) {Ranieri, 2006 #8}. However, for novel anti-angiogenic drugs that do not target VEGF and have different predicted mechanisms of action, an imaging method sensitive to structural changes in the microvasculature independent of changes in vascular permeability would be valuable. Also, DCE-MRI–derived parameters may remain unchanged in the case of microvessel diameter increase and vessel density decrease. In addition, eliminating the high temporal resolution requirement would be beneficial, especially when assessing relatively small tumors and metastases or those subject to physiologic motion such as in the abdomen.

VSI is an alternative approach to assessing microvasculature noninvasively {Dennie, 1998 #27} that exploits the differential dependence of R_2 $(1/T_2)$ and R_2^* $(1/T_2^*)$ relaxation rates on the physical dimensions of microscopic susceptibility distortions. Due to the sensitivity of T_2-MRI to water diffusion, R_2 depends on the vessel size diameter, while R_2^* does not (at clinical field strengths and sufficient susceptibility shift). By measuring changes in these relaxation rates with an intravascular susceptibility contrast agent, estimates for mean microvessel caliber or vessel size index {Tropres, 2001 #32}, vessel density related index (Q) {Jensen, 2000 #30}, and relative blood volume (vascular volume fraction, VVF) can be derived noninvasively. As initially described {Dennie, 1998 #27}, these microstructural estimates are derived by imaging prior to injection of an intravascular magnetic susceptibility contrast agent and at steady-state concentration. The ability to perform steady-state imaging avoids the inevitable tradeoff between high speed and limited resolution/ coverage seen with DCE-MRI and allows acquisition of higher spatial resolution data.

Several groups have demonstrated agreement between VSI-based measurements of tumor mean vessel caliber and microvessel density determined by invasive measurements {Dennie, 1998 #27;Farrar, 2010 #34;Ungersma, 2010 #29} in xenograft models, validating the VSI methodology. Preclinical studies have also demonstrated that VSI metrics are sensitive to the effects of anti-VEGF and anti-angiogenic therapies {Kiselev, 2005 #49;Robinson, 2008 #39;Sampath, 2013 #82;Ungersma, 2010 #29;Zwick, 2009 #36}, providing confidence that this approach may be useful for assessing these targeted therapies clinically. The use of VSI in humans has been limited by the restricted availability of a suitable intravascular contrast agent; several iron-based liver contrast agents have been discontinued in the U.S., leaving no FDA-approved contrast agent available for clinical MRI. Nevertheless, measurements have been made in the brain by means of dynamic imaging with standard low molecular weight gadolinium-based contrast agents {Kiselev, 2005 #49} and customized pulse sequences able to concurrently measure changes in both T_2 and T_2^* {Andre, 2011 #43;Batchelor, 2007

#40;Jensen, 2006 #31;Remmele, 2011 #76;Xu, 2010 #41}, or dual-bolus injections {Hsu, 2009 #44}. However, the dynamic imaging approach to VSI suffers from greater temporal sampling rate requirements compared to DCE-MRI.

Ferumoxytol (Feraheme™, AMAG Pharma Inc., Lexington, MA) is a USPIO (*ultrasmall superparamagnetic iron oxide*) nanoparticles approved to treat iron deficiency anemia in renally insufficient patients. Ferumoxytol has been used preclinically as an intravascular contrast agent, demonstrating sufficient sensitivity to monitor perturbations caused by anti-angiogenic therapies {Gahramanov, 2011 #53;Storey, 2011 #50;Varallyay, 2009 #54}. To date, clinical quantitative MRI with ferumoxytol has focused primarily on evaluating perfusion/permeability in normal brain tissue and CNS lesions {Bjornerud, 2002 #70;Christen, 2012 #55;D'Arceuil, 2013 #61;Dosa, 2011 #58;Dosa, 2011 #57;Fredrickson, 2012 #26;Gahramanov, 2013 #59;Weinstein, 2010 #60;Emblem, 2014 #92;Tropres, 2015 #83}. Making measurements outside of the brain is more difficult because of the effects of respiratory and cardiac motion and susceptibility artifacts, which are especially problematic for echo-planar imaging approaches. Performing VSI in non-brain lesions is of great importance from a drug development perspective, since the majority of patients in Phase 1 oncology trials have advanced systemic metastatic disease with lesions in the chest and abdomen. The liver is a common metastatic site in this patient population, which could be problematic for USPIO-based imaging because Kupffer cells in the surrounding normal liver take up iron oxide nanoparticles; in fact, the liver is the main elimination route of exogenous iron. Persistent relaxivity changes due to the presence of iron oxide nanoparticles in the normal liver aid in the visualization of hepatic lesions, but may limit the ability to make repeat measures of quantitative VSI parameters either before treatment for repeatability studies, or over relatively short time frames (e.g., <48 h) after initiating investigational treatments.

We evaluated the feasibility of acquiring VSI data using ferumoxytol in advanced-stage cancer patients with solid tumors in the body {Fredrickson, 2012 #26}, as part of a multi-center Phase 1 clinical trial of MINT1526A, a novel humanized monoclonal antibody against the $\alpha_5\beta_1$ integrin, an angiogenesis regulator. The primary objective of the trial was to assess safety and tolerability of MINT1526A alone and in combination with the anti-VEGF antibody bevacizumab. The aims of the VSI substudy were to design an imaging protocol using standard product pulse sequences on 1.5T MR scanners to provide measures of VSI parameters; evaluate inter-patient variability of vascular imaging parameters in both normal tissues and solid tumors; gain insights into the time course of contrast changes and the affect on VSI parameters (particularly in liver lesions); and assess translatability by comparing preclinical and clinical VSI measures in both normal and tumor tissue. Finally, we also report on the safety profile of using ferumoxytol as an iron-oxide contrast in a Phase 1 patient cohort.

Methods

Patient Population

Scanning was conducted in 13 patients with advanced-stage solid tumors who were screened for or enrolled in dose-expansion cohorts of a Phase 1 clinical trial of MINT1526A. To be

included in the imaging component of the trial, patients had to have a lesion of greater than 3 cm in the longest dimension in the liver, or 2 cm in other metastatic sites. Exclusion criteria were: known hypersensitivity to ferumoxytol or any of its components, current or recent (within past 3 months) administration of ferumoxytol or similar iron substitute, evidence of iron overload (including but not limited to known hemochromatosis, chronic hemolysis, or chronic blood transfusions), requirement for diagnostic MRI for disease monitoring and/or clinical management (e.g., due to known intolerability to CT contrast agent), and conventional contraindications to MRI.

Two scans were acquired during the trial screening period, prior to the start of study drug. The first scan included a ferumoxytol injection, while the second scan (~48 h after the first scan) evaluated delayed effects of the prior ferumoxytol injection. Two additional scans, again with and without ferumoxytol injection and 48 h apart, were acquired after 2 weeks of study treatment (Day 15 scans). Only limited on-treatment data is included here, as the focus of this manuscript is on the VSI implementation. All protocols were approved by the local Institutional Review Boards (IRB) where imaging was performed.

Clinical Imaging Protocols

Clinical imaging protocols were implemented on two Siemens (Symphony, Espree) and one GE Signa 1.5T MR scanners at three different imaging centers, using stock pulse sequences. Standard spine and torso phased-array coils were used for signal reception, positioned to provide coverage of the target lesion(s) previously identified on diagnostic CT scans. All images were acquired in the transverse plane. A dual-echo multi-slice turbo spin-echo (TSE) T_2-weighted sequence (pulse repetition time (TR) 2600 ms, echo times (TE) 6 and 96 ms, echo train length 15) was used to derive maps of the estimated transverse relaxation rate, R_2. R_2^* maps were created based on a six-echo multi-slice spoiled gradient-echo T_2^*-sequence (TR 170 ms, TE 3.4–39 ms). Scan parameters for both sequences were selected to maintain acquisition times within 15–20 s breath-holds to reduce motion artifacts In order to acquire 15–20 6-mm trans-axial slices, 2–5 breath-holds were required for each sequence. Data for R_2 and R_2^* maps were acquired both before and again starting 5 min after ferumoxytol injection. A 3 mg Fe/kg dose of ferumoxytol diluted 1:1 with saline was injected at 2 mL/sec using a power injector, followed by a saline flush. This dose was chosen to be within the lower range of literature reported ferumoxytol doses {Neuwelt, 2009 #81;Varallyay, 2013 #80} in order to facilitate repeat studies and addressed recent safety concerned by FDA-issued black box. Ferumoxtyol was injected during the first scan prior to study drug administration, and during the third scan, after 2 weeks of treatment. Pre-injection diffusion-weighted images (b=0,200,800 s/mm^2 for each of the 3 principal magnet axes, TR ~3000 ms, TE ~95 ms, 8 averages, free-breathing) were also acquired, and used to calculate apparent diffusion coefficient (ADC) maps using mono-exponential curve fitting. Additional imaging included anatomical scans (fast imaging with steady-state precession, FISP/FIESTA), T_1-weighted and multi-flip angle T_1-mapping scans. The total scan time was approximately 30 min.

Clinical Image Analysis

Multi-echo data were fitted to mono-exponential models to derive voxel-wise R_2 and R_2^* maps using MRVision software (MRVision Co., Redwood City, CA) at each imaging timepoint. Images were then spatially registered across timepoints using manual rigid body translations, to visually best match the target lesion(s). This procedure primarily corrects for slight variations in diaphragm position from scan to scan. Difference maps (ΔR_2 and ΔR_2^*) were derived, which are proportional to microvascular and total blood volume, respectively. Maps of the vessel density related index {Jensen, 2000 #30}, Q= $\Delta R_2/(\Delta R_2^*)^{2/3}$, were also generated. These three metrics were selected as they are amongst the simplest (and therefore likely the most robust) VSI-related metrics. Measurements were made in renal cortex, liver, muscle (typically in the muscle mass close to the vertebral column), and blood pool (generally descending aorta), if these regions were available within the scan FOV for each patient. One to three target lesions were also evaluated per patient. For each measurement, ROIs were defined manually across several slices, avoiding any areas with obvious image artifacts due to motion or field inhomogeneity. Lesion ROI selection was guided by diffusion-weighted images and ADC maps; lesions or areas of lesions with relatively low ADC values (usually $<\sim 1.2 \times 10^{-3}$ mm^2/s) were preferentially selected. To simplify the analysis and remove potential errors due to multiple registration steps, ΔR_2^*, ΔR_2, and Q parameters were also calculated from the median R_2 and R_2^* values within whole-lesion ROIs, and compared to registered image-derived values. Repeatability of these measurements was assessed by comparing screening and Day 15 data in renal cortex, assuming normal tissues are essentially unaffected by treatment.

Relationship of $\Delta R_2^*_{tissue}$ and Blood Ferumoxytol Concentration—When deriving relative blood volumes from steady-state susceptibility contrast data with an intravascular contrast agent, a fundamental assumption is that changes in $\Delta R_2^*_{tissue}$ are linearly related to the tissue concentration of the contrast agent. This has been shown in preclinical models {Bjornerud, 2002 #70;Tropres, 2001 #32}; Bjørnerud et al. {Bjornerud, 2002 #70} additionally showed that change in blood ($\Delta R_2^*_{Blood}$) is quadratically related to contrast agent concentration in a pig model with another USPIO agent, Clariscan™. Using ferumoxytol, similar relationships were shown in human gray and white matter and the sagittal sinus {Dosa, 2011 #57}.

With only one bolus dose of ferumoxytol in our protocol and no direct measures of contrast agent concentration, these described relationships could not be directly evaluated in our study. However, we were able to observe these relationships to some extent. The correlation between the square root of $\Delta R2^*_{Blood}$ and the blood concentration of Fe was first confirmed; the concentration was calculated as the injected dose of Fe divided by the total blood volume estimated using the Nalder Method {Nalder, 1962 #84} for each subject. The square root of $\Delta R_2^*_{blood}$ as a surrogate for blood concentration was then plotted against $\Delta R_2^*_{tissue}$ for all subjects, with *tissue* representing renal cortex, liver, muscle, and lesion.

Relationship between $\Delta R_2^*_{tissue}$, $\Delta R_2{}_{tissue}$, and Q—While measures of ΔR_2^* and ΔR_2 are both dependent on contrast agent concentration, the relationship between ΔR_2^* and ΔR_2 has been shown to be approximately linear and varies with tissue type, and the quantity

Q is independent of contrast agent concentration and will therefore show little dependence on R_2* {Jensen, 2000 #30}. We evaluated these relationships in our data by examining both $R_{2tissue}$ and Q as a function of R_2*_{tissue} in tumor and normal renal cortex, both in voxel-based and whole-ROI measurements.

Preclinical Imaging

Four athymic nude mice bearing human tumor xenografts of colorectal origin (HM-7) were imaged 10 days after inoculation. Tumor volumes, measured by caliper at the time of imaging, were 150–250 mm^3. All animal procedures were approved by the Association for Assessment and Accreditation of Laboratory Animal Care–accredited Genentech review board.

VSI-MRI was performed on a 4.7T Varian Unity Inova MRI system with a 20 mm two-loop surface coil. Eight coronal, 1-mm-thick slices were acquired with a 25.6×25.6 mm FOV and 64×64 (ADC, T_2) or 128×128 (T_2*) matrix. A multi-slice, diffusion-weighted fast spin-echo imaging sequence was used to obtain ADC measurements (6 b-values from 82–1129 s/mm^2, TR 3 s, echo train length 4, 2 averages, δ 3.3 ms, 30 ms). R_2 and M_0 maps were acquired using a multi-slice, single-echo spin-echo imaging sequence (TE 5, 26, 47, 68 ms, TR 3 s and 1 average) and R_2* maps were acquired using a multi-echo, multi-slice gradient echo sequence (TE 5, 10, 15, 20, 25, 30, 35, 40 ms, TR 345 ms and 4 averages) prior to and 3 min post-injection of ferumoxytol (6 mg Fe/kg via tail-vein catheter). The higher dose of iron was used in the murine model, as compared to human dose, due to rapid ferumoxytol kinetic in rodents and based on previous reports.

VSI MRI parameters were calculated voxel-by-voxel in the viable tumor tissue using the pre- and post-contrast R_2 and R_2* maps and ADC maps in a multispectral approach {Berry, 2008 #90;Carano, 2004 #88}. Muscle ROIs were drawn manually on the neighboring quadriceps muscle, also present in the imaging FOV. Imaging was conducted at a single session, without the administration of any study drug.

Estimation of Relative Vascular Volume Fraction—Vascular volume fraction (VVF) was calculated from measured R_2* values as previously described {Jensen, 2000 #30;Tropres, 2001 #32} using the following equation:

$$VVF = \frac{3}{4\pi} \frac{\Delta R_2^*}{\gamma \Delta \chi B_0}$$

Since it was not possible to measure the susceptibility difference (χ) in patients as part of the clinical trial, the ratio of VVF in tumor to VVF in normal tissue (muscle) was calculated, which simplifies to the ratio of R_2* in tumor to R_2* in muscle for each subject. The same ratio was also calculated using mouse data, and summary ratios were compared to the relative measures in humans. Assuming the same intravascular iron oxide agent is used, a scaling factor was needed to compare values across species {Tropres, 2001 #32}:

$$Relative\ VVF = \frac{\Delta R_2^{*mouse}}{\Delta R_2^{*human}} \frac{\left[Iron\ Dose_{human}(mg/kg) \Big/ Total\ Blood\ Vol_{human}\,(ml/kg) \right]}{\left[Iron\ Dose_{mouse}(mg/kg) \Big/ Total\ Blood\ Vol_{mouse}\,(ml/kg) \right]}$$

Data and Statistical Analysis

Data are presented as mean ± standard deviation (SD). Correlations were evaluated in R {, 2013 #91}. with a significance level of $p<0.05$. A paired t-test assuming equal variance was used for comparisons between individual patient data at multiple timepoints.

Results

Clinical Data: Image Analysis

Nine patients with metastatic disease (4 colorectal cancer, 2 carcinoid, ovarian, osteosarcoma, and bladder cancer) completed the full imaging protocol and provided evaluable data. An additional 4 patients received ferumoxytol and participated in one or two scans during the screening period, but were screen failures for the trial because of non-imaging eligibility criteria, or terminated early. A total of 17 lesions (11 liver, 2 peritoneal, 2 lung, mesenteric, and renal) were suitable for analysis. No adverse events related to ferumoxytol injection were reported.

Representative histograms from one patient (Figure 1) show a marked increase in R_2 immediately following ferumoxytol injection in all tissues. By 48 h post-injection, R_2 had returned to baseline in the renal cortex and partially recovered in the lesion and normal liver.

The time course of R_2 and R_2^* changes in muscle, liver, renal cortex, and blood pool are summarized as mean (± SD) in Figure 2. Measurements in each tissue were possible in most, but not all patients, because of the required placement of the imaging FOV relative to tumor. Also, R_2 could not be measured in the blood in the aorta due to the spin-echo sequence used. Post-injection, the mean increase in R_2 was 121% ± 58% and 79% ± 41% in liver and renal cortex, respectively, which returned to 61% ± 18% and 42% ± 41% above baseline by 48 h. R_2^* increased by 612% ± 304% and 568% ± 253% in liver and renal cortex, and returned to 189% ± 111% and 102% ± 113% above baseline by 48 h. The liver signal was the most variable, likely reflecting different iron and fat content, and variable uptake and retention of iron oxide across the population. Measurements in muscle were variable across patients, but as expected, changes with contrast administration were comparatively small. All post-contrast increases in liver, renal cortex, muscle, and blood were significant ($p<0.005$). By 48 h, changes in liver R_2 and R_2^* relative to pre-contrast were still significant ($p<0.005$), as were renal cortex R_2 and blood R_2^* ($p<0.05$). Similar patterns of change were seen on Day 15 scans for all normal tissue. R_2 and R_2^* values on Day 15 prior to contrast administration in liver, renal cortex, muscle, and blood were not significantly different than the pre-contrast values measured at screening, based on paired t-tests ($p>0.05$).

Representative CT and T_2-weighted MRI images acquired before and after ferumoxytol injection in a colorectal cancer patient are shown in Figure 3a–c; the heterogeneity of the

multiple liver lesions can be appreciated in the post-contrast image. Maps of R_2, R_2^*, Q, and ADC are also shown for the same patient (Figure 3d–g); the core of the large central lesion is necrotic with high ADC. For quantitative analysis, we measured the offshoot of the lesion with relatively low ADC (0.98×10^{-3} mm^2/s), as indicated on the R_2 map. Some artifacts appear on the right side of the images due to local mis-registration of the liver across multiple breath-holds.

Repeatability of VSI metrics in tumors could not be directly assessed given the lack of double-baseline measurements in our protocol. However, by assuming normal tissues such as the renal cortex are not affected by treatment, comparisons between screening and Day 15 data served as an approximation. The repeatability of R_2, R_2^*, and Q in the renal cortex, as measured by the coefficient of variation (CV%) derived from the paired screening and Day 15 scans from each subject, ranged from 12.3 to 14%, while the CV% for ADC was 4.9% (Figure 4); these CV% values are consistent with those reported for other MRI-based vascular metrics, such as K_{trans} {Tofts, 1999 #48}. Side-by-side comparisons of screening and Day 15 results for both ADC and Q measurements paired by patient are also shown.

Plots of the time course of R_2 and R_2^* in individual lesions are shown in Figure 5, grouped by lesion location. Post-injection, the mean increase in R_2 was 34% ± 16% (p<0.005) which dropped to 29% ± 22% (p<0.005) above baseline by 48 h; R_2^* increased by 182% ± 90% (p<0.005) and returned to 72% ± 49% (p<0.005) above baseline by 48 h. The persistent increase in R_2 at 48 h (indeed progressive increase in some lesions) contrasts to the near complete recovery of R_2 in blood and renal cortex. The persistent increases at 48 h may be due to accumulation of contrast agent due to extravasation, or uptake by macrophages within a lesion. While there was significant variability in R_2 value between lesions, the relative change following ferumoxytol was quite consistent. The two lung lesions had much higher R_2^* values at baseline (Figure 5b), which may be indicative of hemorrhagic necrosis; however, overall, the percent changes post-injection were similar to changes seen in liver and pelvic lesions.

Median values of R_2, R_2^*, Q, and ADC are shown for each target lesion in Figure 6. One liver lesion had a very high R_2^*; this was likely due to inclusion of normal liver tissue with the ROI given the location and size of the lesion. Note that the most necrotic lesion (highest ADC value) also had the lowest Q value. Q values in normal renal cortex were quite consistent across patients, in comparison to the heterogeneity in tumor Q. Not surprisingly, variability in Q across tumors appeared to be mostly driven by variation in R_2.

Clinical Data: Model-Generated Comparisons

As shown in Figure 7, the correlation between $\sqrt{\Delta R_{2*\text{blood}}}$ and the contrast agent blood concentration, calculated for each subject as the injected dose of Fe divided by the total blood volume estimated using the Nalder Method, was significant ($r^2 = 0.62$, p<0.02), indicating $\sqrt{\Delta R_{2*\text{blood}}}$ is a reasonable surrogate for blood contrast agent concentration. Figure 7 also shows the relationship between $\sqrt{\Delta R_{2*\text{blood}}}$ and $R_2^*_{\text{tissue}}$ for renal cortex, muscle, liver, and lesions. As expected, linear trends were seen in normal tissue, particularly for the higher blood volume renal cortex. While the values for K_{tissue} ($K_{\text{tissue}} =$

$R_2^*_{tissue}/C_p$, where C_p is the contrast agent concentration, or in our case, $\sqrt{\Delta R_{2*blood}}$) derived from our data cannot be directly compared to values reported by Bjornerud {Bjornerud, 2002 #70} since different iron-oxide agents were used, the ratio between the same tissue types is similar: $K_{renal\ cortex}/K_{muscle}$ = 14.8, Bjørnerud $K_{renal\ cortex}/K_{muscle}(101/6.5)$ = 15.5 {Carano, 2004 #88}. The lack of relationship seen with lesion R_2^* may simply reflect the wide variability in tumor vascular geometry in the lesions evaluated. The required assumption that the contrast agent remains compartmentalized may also not hold true in the liver.

The dependence of ΔR_2 and Q on ΔR_2^* in lesions and renal cortex (Figure 8) is based on whole-ROI analyses as well as for individual voxels from one liver lesion in a patient with metastatic colorectal cancer. As anticipated based on Jensen's results {Jensen, 2000 #30}, there is an approximately linear relationship between ΔR_2 and ΔR_2^*, while Q is relatively insensitive to changes in ΔR_2^*, indicating lack of dependence on contrast agent concentration.

ΔR_2 and ΔR_2^* measurements from parametric maps derived from registered images were compared to results generated from the simplified whole-lesion ROI for all target lesions. The correlation between the two approaches was very high (r^2 = 0.98); the simplified approach yields very similar values compared to the image-based method, though at the cost of losing information on heterogeneity within the ROI. Similar findings were also seen for the derived vessel density-related parameter, Q.

Preclinical Comparison

Figure 9 shows representative maps (ADC, ΔR_2, ΔR_2^*, and Q) from a xenograft tumor; the qualitative relationships between parameters are similar to those seen for the lesions in our patient cohort. Plots of ΔR_2, ΔR_2^*, and Q are also shown for both mouse and human tumors. Differences in the relaxation rate changes between human and mouse measurements likely reflect methodological differences (field strength 1.5T vs. 4.7T), different pulse sequences (multi-echo vs. incremented spin-echo T_2 measurement), and manual tumor segmentation vs. automated segmentation of viable xenograft tissue using a multispectral approach {Ungersma, 2010 #29}. Variability in both ΔR_2 and ΔR_2^* was much higher across the human subjects, which may be expected given a Phase I population and lesion location heterogeneity in comparison to xenograft models. However, it is interesting to note that the variability in Q across the human subjects was more consistent with the mouse measures. Median tumor Q in mice was about twice the median Q in human tumors. This may reflect a true increased vessel density due to the subcutaneous nature of flank xenograft models, though results are also likely affected by better segmentation of mouse tumors compared to human tumors, and other methodological differences such as field strength and pulse sequence details.

The median relative VVF of the HM-7 flank xenograft tumors compared to quadriceps muscle in mice was 1.4, indicating a 40% increase in VVF in tumors compared to VVF in muscle. This is in the range of what might be expected given the VVF values reported in the literature for mouse muscle VVF (1.89%[35]) and various xenograft tumor models (2.1%–

6.6%[35] and 0.8%–3.24%[36,37]). Assuming a total blood volume of 70 mL/kg, the median relative VVF in mouse muscle compared to human muscle was estimated as $(11.8\ s^{-1}/5.7\ s^{-1})*(3\ mg/kg\ Fe/6\ mg/kg\ Fe) = 1.0$, indicating that measured muscle blood volumes are similar between species. The median relative VVF of tumors compared to muscle in humans was 4.9, indicating a higher relative blood volume in tumors compared to muscle in humans, as well as higher relative blood volumes in human tumors (~9%) compared to xenograft tumors.

Discussion

While DCE-MRI is well-suited for therapies that target the VEGF pathway because of its sensitivity to alterations in vascular permeability, the development of therapies that induce structural changes unrelated to permeability would benefit from robust in vivo measures of microvascular structure. The clinical availability of an intravascular contrast agent with a relatively long half-life allows the expansion of available tools for the assessment of new oncologic therapies with a range of anti-angiogenic mechanisms of action. The data in this study demonstrate the feasibility of evaluating tumor vasculature in metastatic lesions throughout the body using the USPIO agent ferumoxytol as an intravascular contrast agent and standard product pulse sequences on commercial MRI scanners. Operationally, there were minimal hurdles to including the use of ferumoxytol as part of the investigative study; most of the clinical sites already had general experience with ferumoxytol as a therapy for anemia in their oncology patients, and no additional IRB reviews were required.

We observed no adverse events related to ferumoxytol injection. However since completion of our study, the US Food and Drug Administration strengthened its existing safety warning on the Feraheme label, reflecting continued post-marketing observations of severe adverse events. Most gadolinium contrast agents also carry such a 'black box' warning which highlight potential risks but do not account for possible benefits of using these agents, such as more accurate diagnosis and therapy selection. We believe that VSI using ferumoxytol will ultimately be shown to convey a similar benefit to patients which will outweigh the low risk of anaphylaxis. Nevertheless the recent FDA warning underlines the need to closely monitor patients receiving ferumoxytol while in the magnet as well as afterwards and to ensure adequate acute care is available for any adverse events. In this study, we have purposively chosen the low injection doses for ferumoxytol; in addition, each patient was monitored 60-min post-injection for any signs of possible anaphylactic reactions.

Overall, image quality was sufficient for analysis. Though artifacts due to patient motion were present in some scans, it did not preclude measurements in the tumors. At a minimum, a multi-echo gradient echo sequence is needed for R_2^* measurement, which may not be available on some older scanners. The use of a blood-pool contrast agent allows for steady-state imaging with slower temporal and higher spatial resolution sequences. This is counterbalanced by the requirement of maintaining individual acquisitions within a reasonable breath-holding duration and obtaining full coverage of target lesions(s) along with relevant normal tissue. These considerations tended to increase total acquisition times in the current protocol. While breath-holding minimized motion artifacts in the scans, spatial registration across multiple series is required to calculate VSI parameters, and this proved

challenging in some cases where lesions were small or the diaphragm position changed markedly between individual breath-holds.

The necessity of breath-holding for scanning abdominal lesions also dictated the use a of a turbo spin-echo sequence for estimating R2. Further, both short and long TE images must be acquired in the same breath-hold, since acquiring them in sequential breath-holds results in noisy R2 and ΔR_2 estimates due to even small spatial registration errors. Though we optimized the TSE parameters as far as possible to achieve reasonable coverage over a small number of breath-holds, this still resulted in a 7–10ms echo spacing. A short echo spacing in the TSE echo train inevitably results in reduced sensitivity to diffusion driven spin dephasing within the magnetic susceptibility gradients around microvessels, which is a key component of the VSI model {Tropres, 2015 #83}. As a result we likely underestimate ΔR_2 changes due to ferumoxytol injection. One solution to this problem is the use of spin-echo EPI sequences. Multi-shot T_2-weighted echo planar imaging is available on most modern scanners and this generates a rapid long-TE spin-echo image, however these sequences typically do not yet allow generation of both short and long TE images required to calculate R2 within a single breath-hold. Another challenge with EPI is the narrow phase-encode bandwidth which can result in significant phase-encode direction blurring after the injection of susceptibility contrast agents, which is problematic for small structures. Nevertheless the use of more efficient novel EPI sequences for measuring changes in T_2 and T_2* simultaneously {Andre, 2011 #43;Batchelor, 2007 #40;Jensen, 2006 #31;Remmele, 2011 #76;Xu, 2010 #41} may be ideal for making VSI measurements with USPIOs, if used in multi-shot rather than single-shot mode. Another limitation of our methodology is the relatively noisy measurement of R2* in whole blood after ferumoxytol injection. Even with dilution of the injection volume with saline, R2* was difficult to measure in whole blood because the TE values used in our gradient echo sequence were optimized of tumor measurements. In future, the inclusion of an additional gradient echo acquisition with much shorter TE values would allow more accurate estimates of tumor blood volume by better characterizing the magnetic susceptibility shift in whole blood.

Our intention in this study was to evaluate the feasibility for clinical VSI using currently available pulse sequences in the challenging setting of imaging abdominal tumors. As multi-echo multi-shot EPI based sequences are more widely implemented on clinical scanners, the accuracy of these VSI metrics in organs outside of the head will likely improve.

The problem of spatial mis-registration errors when calculating VSI metrics from multiple input images and multiple breath-holds can be addressed by the calculation of median tumor values from the individual (pre-, post-contrast R_2 and R_2*), which can then be used to calculate a single value for average tumor Q or blood volume. This approach produced values in excellent agreement with median values measured from registered Q and ΔR_2* maps, suggesting it is sufficient for quantifying average tumor properties. In addition, our approach to ROI definition tended to define fairly homogeneous-appearing tumor regions by using diffusion scans to avoid regions of obvious necrosis or hemorrhage.

These data were consistent with the theory of microvascular imaging and experimental findings of previous investigators[4]. Although our protocol used a fixed mg/kg contrast agent

dose, we observed linear relationships between R_2*_{tissue} and contrast agent concentration in each subject, either calculated from total blood volume estimates or $\sqrt{\Delta R_{2*}}$ measured in blood. We also observed a linear relationship between R_2 and R_2* in tumor and normal tissue, and most importantly, found that Q was relatively independent of R_2* and therefore contrast agent concentration. These results provide further support that Q is a promising biomarker, even in the heterogeneous setting of Phase I clinical trials of anti-angiogenic therapies enrolling patients with diverse solid tumors.

The high level of ferumoxytol accumulation in the liver did not prevent the measurement of VSI metrics in hepatic metastases. Close inspection of the images revealed that the boundaries of liver lesions were well defined on scans both immediately post-injection and 48 h post-injection. On the 48 h image, markedly elevated relaxation rates were still present in tumors and liver, while blood and renal cortex values returned closer to baseline. Based on the ~15 h plasma half-life of ferumoxytol in humans, about 10% of the original blood contrast agent concentration should remain after 48 h; accordingly, measurements of R_2* and R_2 were slightly above baseline values in the blood pool and renal cortex at that timepoint. Sustained elevation of R_2* and R_2 in liver at 48 h may be due to extravasation of the contrast agent and uptake by Kupffer cells. In tumors, R_2* remained above baseline at 48 h, though below immediate post-contrast levels, while R_2 at 48 h was similar to the immediate post-contrast value and in some cases increased further. This is likely due to delayed leakage of ferumoxytol into the tumor extravascular space, which likely has much larger micro-vascular (R_2) than macro-vascular (R_2*) relaxation effects. In addition, regional R_2 elevation in experimental breast tumor xenografts at 24 h post-ferumoxytol injection has been attributed to uptake by tumor-associated macrophages {Daldrup-Link, 2011 #79}, which may explain some of the progressive increase in R_2 seen in several tumors. It is possible that inclusion of the T1 measurements in tumor core and periphery may yield additional insight into whether delayed uptake of ferumoxytol is due to slow vascular extravasation or uptake into tumor associated macrophages, however this issue is beyond the scope of the current paper.

A limitation of this study was the lack of double-baseline measurements to determine repeatability of these metrics in a clinical trial setting. However, it is encouraging to note that measures made in the renal cortex at screening and Day 15 were consistent across subjects, with CV% less than 15%. Measurements in lesions at Day 15 were not reported, as there were no clear trends in the small group of patients studied, many of whom were rapidly progressing with tumor size changes seen within a 2-week window.

While we do not have invasive measurements of tumor vessel density in these patients, previous preclinical studies have shown good agreement between MRI-derived metrics and microvessel density measured by microCT {Ungersma, 2010 #29}. Comparisons to preclinical data in this study show that estimates of Q are similar, though potentially slightly lower in human lesions compared to the xenograft models, while the variability of Q measurements are similar overall. Relative VVF measured in muscle was similar in mouse and humans, while relative blood volumes were about 3.5 times higher in human tumors compared to HM-7 xenograft tumors. Though we were not able to calculate absolute VVF values, relative values may still be useful, particularly when evaluating changes in VVF after

treatment. Therefore, both relative VVF and Q may be viable markers of effect when studying anti-angiogenic therapies. More quantitative estimates of tumor microvessel density and vessel caliber are possible but require measurement of tumor diffusion coefficient and magnetic susceptibility shift {Jensen, 2006 #31;Tropres, 2004 #28}. While we did measure ADC, an assessment of the blood susceptibility shift would require a more accurate blood R_2^* measurement from a large vessel. Moreover calculation of such metrics would be more valuable future clinical studies that include tumor biopsies, allowing validation of these *in vivo* VSI metrics against invasive measurements of tumor vasculature.

Conclusions

Unlike DCE-MRI, the VSI approach does not rely on contrast agent extravasation or high temporal resolution imaging and may prove valuable for assessing novel anti-angiogenic therapies that may not affect vascular permeability. Clinical VSI is feasible in a multi-center study of patients with lesions outside the brain, using standard MRI techniques and ferumoxytol as a contrast agent. Iron oxide contrast agent accumulation in the liver does not preclude measurement of VSI parameters in liver metastases. We observed no adverse site effects of repetitive ferumoxytol injection at 3 mg Fe/kg intravenous doses. A repeatability study is needed to establish test-retest variability, which in turn may be used to determine treatment changes in future trials of anti-angiogenic therapies.

Acknowledgments

References

1. O'Connor JP, Jackson A, Parker GJ, Roberts C, Jayson GC. Dynamic contrast-enhanced MRI in clinical trials of antivascular therapies. Nat Rev Clin Oncol. 2012; 9:167–177. [PubMed: 22330689]

2. Tofts PS, Brix G, Buckley DL, et al. Estimating kinetic parameters from dynamic contrast-enhanced T(1)-weighted MRI of a diffusable tracer: standardized quantities and symbols. J Magn Reson Imaging. 1999; 10:223–232. [PubMed: 10508281]

3. Ranieri G, Patruno R, Ruggieri E, Montemurro S, Valerio P, Ribatti D. Vascular endothelial growth factor (VEGF) as a target of bevacizumab in cancer: from the biology to the clinic. Curr Med Chem. 2006; 13:1845–1857. [PubMed: 16842197]

4. Dennie J, Mandeville JB, Boxerman JL, Packard SD, Rosen BR, Weisskoff RM. NMR imaging of changes in vascular morphology due to tumor angiogenesis. Magn Reson Med. 1998; 40:793–799. [PubMed: 9840821]

5. Tropres I, Grimault S, Vaeth A, Grillon E, Julien C, Payen JF, Lamalle L, Decorps M. Vessel size imaging. Magn Reson Med. 2001; 45:397–408. [PubMed: 11241696]

6. Jensen JH, Chandra R. MR imaging of microvasculature. Magn Reson Med. 2000; 44:224–230. [PubMed: 10918321]

7. Farrar CT, Kamoun WS, Ley CD, Kim YR, Kwon SJ, Dai G, Rosen BR, di Tomaso E, Jain RK, Sorensen AG. In vivo validation of MRI vessel caliber index measurement methods with intravital optical microscopy in a U87 mouse brain tumor model. Neuro Oncol. 2010; 12:341–350. [PubMed: 20308312]

8. Ungersma SE, Pacheco G, Ho C, Yee SF, Ross J, van Bruggen N, Peale FV Jr, Ross S, Carano RA. Vessel imaging with viable tumor analysis for quantification of tumor angiogenesis. Magn Reson Med. 2010; 63:1637–1647. [PubMed: 20512867]

9. Kiselev VG, Strecker R, Ziyeh S, Speck O, Hennig J. Vessel size imaging in humans. Magn Reson Med. 2005; 53:553–563. [PubMed: 15723391]

10. Robinson SP, Ludwig C, Paulsson J, Ostman A. The effects of tumor-derived platelet-derived growth factor on vascular morphology and function in vivo revealed by susceptibility MRI. Int J Cancer. 2008; 122:1548–1556. [PubMed: 18033683]

11. Sampath D, Oeh J, Wyatt SK, et al. Multimodal microvascular imaging reveals that selective inhibition of class I PI3K is sufficient to induce an antivascular response. Neoplasia. 2013; 15:694–711. [PubMed: 23814482]

12. Zwick S, Strecker R, Kiselev V, et al. Assessment of vascular remodeling under antiangiogenic therapy using DCE-MRI and vessel size imaging. J Magn Reson Imaging. 2009; 29:1125–1133. [PubMed: 19388117]

13. Andre, JB., Schmiedeskamp, H., Zaharchuk, G., Straka, M., Christen, T., Recht, L., Bammer, R. Initial experience with vessel size imaging in recurrent glioblastoma multiforme using a multiple spin and gradient echo (SAGE) perfusion bolus contrast sequence. Proceedings of the 19th Annual Meeting of ISMRM; Montreal, Canada. 2011; Abstract 2428

14. Batchelor TT, Sorensen AG, di Tomaso E, et al. AZD2171, a pan-VEGF receptor tyrosine kinase inhibitor, normalizes tumor vasculature and alleviates edema in glioblastoma patients. Cancer Cell. 2007; 11:83–95. [PubMed: 17222792]

15. Jensen JH, Lu H, Inglese M. Microvessel density estimation in the human brain by means of dynamic contrast-enhanced echo-planar imaging. Magn Reson Med. 2006; 56:1145–1150. [PubMed: 17029231]

16. Remmele S, Ring J, Senegas J, Heindel W, Mesters RM, Bremer C, Persigehl T. Concurrent MR blood volume and vessel size estimation in tumors by robust and simultaneous DeltaR2 and DeltaR2* quantification. Magn Reson Med. 2011; 66:144–153. [PubMed: 21305604]

17. Xu, C., Schmidt, W., Brunecker, P., Kisilev, V., Gall, P., Bodammer, N., Fieback, J. The assessment of vessel size index and its application in patients with ischemic stroke. Proceedings of the 18th Annual Meeting of ISMRM; Stockholm, Sweden. 2010; Abstract 648

18. Hsu YY, Yang WS, Lim KE, Liu HL. Vessel size imaging using dual contrast agent injections. J Magn Reson Imaging. 2009; 30:1078–1084. [PubMed: 19856441]

19. Gahramanov S, Raslan AM, Muldoon LL, Hamilton BE, Rooney WD, Varallyay CG, Njus JM, Haluska M, Neuwelt EA. Potential for differentiation of pseudoprogression from true tumor progression with dynamic susceptibility-weighted contrast-enhanced magnetic resonance imaging using ferumoxytol vs. gadoteridol: a pilot study. Int J Radiat Oncol Biol Phys. 2011; 79:514–523. [PubMed: 20395065]

20. Storey P, Ji L, Li LP, Prasad PV. Sensitivity of USPIO-enhanced R2 imaging to dynamic blood volume changes in the rat kidney. J Magn Reson Imaging. 2011; 33:1091–1099. [PubMed: 21509866]

21. Varallyay CG, Muldoon LL, Gahramanov S, Wu YJ, Goodman JA, Li X, Pike MM, Neuwelt EA. Dynamic MRI using iron oxide nanoparticles to assess early vascular effects of antiangiogenic versus corticosteroid treatment in a glioma model. J Cereb Blood Flow Metab. 2009; 29:853–860. [PubMed: 19142191]

22. Pohlmann A, Karczewski P, Ku MC, et al. Cerebral blood volume estimation by ferumoxytol-enhanced steady-state MRI at 9.4 T reveals microvascular impact of alpha1 -adrenergic receptor antibodies. NMR Biomed. 2014; 27:1085–1093. [PubMed: 25060359]

23. Bjornerud A, Johansson LO, Briley-Saebo K, Ahlstrom HK. Assessment of T1 and T2* effects in vivo and ex vivo using iron oxide nanoparticles in steady state--dependence on blood volume and water exchange. Magn Reson Med. 2002; 47:461–471. [PubMed: 11870832]

24. Christen T, Ni W, Qiu D, Schmiedeskamp H, Bammer R, Moseley M, Zaharchuk G. High-resolution cerebral blood volume imaging in humans using the blood pool contrast agent ferumoxytol. Magn Reson Med. 2012; 70:705–710. [PubMed: 23001902]

25. D'Arceuil H, Coimbra A, Triano P, Dougherty M, Melo J, Moseley M, Glover G, Lansberg M, Blankenberg F. Ferumoxytol enhanced resting state fMRI and relative cerebral blood volume mapping in normal human brain. Neuroimage. 2013; 83:200–209. [PubMed: 23831413]

26. Dosa E, Guillaume DJ, Haluska M, Lacy CA, Hamilton BE, Njus JM, Rooney WD, Kraemer DF, Muldoon LL, Neuwelt EA. Magnetic resonance imaging of intracranial tumors: intra-patient comparison of gadoteridol and ferumoxytol. Neuro Oncol. 2011; 13:251–260. [PubMed: 21163809]

27. Dosa E, Tuladhar S, Muldoon LL, Hamilton BE, Rooney WD, Neuwelt EA. MRI using ferumoxytol improves the visualization of central nervous system vascular malformations. Stroke. 2011; 42:1581–1588. [PubMed: 21493906]

28. Gahramanov S, Muldoon LL, Varallyay CG, Li X, Kraemer DF, Fu R, Hamilton BE, Rooney WD, Neuwelt EA. Pseudoprogression of glioblastoma after chemo- and radiation therapy: diagnosis by using dynamic susceptibility-weighted contrast-enhanced perfusion MR imaging with ferumoxytol versus gadoteridol and correlation with survival. Radiology. 2013; 266:842–852. [PubMed: 23204544]

29. Weinstein JS, Varallyay CG, Dosa E, Gahramanov S, Hamilton B, Rooney WD, Muldoon LL, Neuwelt EA. Superparamagnetic iron oxide nanoparticles: diagnostic magnetic resonance imaging and potential therapeutic applications in neurooncology and central nervous system inflammatory pathologies, a review. J Cereb Blood Flow Metab. 2010; 30:15–35. [PubMed: 19756021]

30. Emblem KE, Farrar CT, Gerstner ER, Batchelor TT, Borra RJ, Rosen BR, Sorensen AG, Jain RK. Vessel caliber--a potential MRI biomarker of tumour response in clinical trials. Nat Rev Clin Oncol. 2014; 11:566–584. [PubMed: 25113840]

31. Tropres I, Pannetier N, Grand S, Lemasson B, Moisan A, Peoc'h M, Remy C, Barbier E. Imaging the microvessel caliber and density: principles and applications of microvascular MRI. Magn Reson Med. 2015; 73:325–341. [PubMed: 25168292]

32. Fredrickson, J., Serkova, N., Carano, RA., Wyatt, S., Pirzkall, A., Weekes, C., Silverman, JM., Rosen, L., de Crespigny, A. Clinical translation of VSI using ferumoxytol: feasibility in a phase I oncology clinical trial population. Proceedings of the 20th Annual Meeting of ISMRM; Melborne, Australia. 2012; Abstract 1987

33. Neuwelt EA, Hamilton BE, Varallyay CG, Rooney WR, Edelman RD, Jacobs PM, Watnick SG. Ultrasmall superparamagnetic iron oxides (USPIOs): a future alternative magnetic resonance (MR) contrast agent for patients at risk for nephrogenic systemic fibrosis (NSF)? Kidney Int. 2009; 75:465–474. [PubMed: 18843256]

34. Varallyay CG, Nesbit E, Fu R, Gahramanov S, Moloney B, Earl E, Muldoon LL, Li X, Rooney WD, Neuwelt EA. High-resolution steady-state cerebral blood volume maps in patients with central nervous system neoplasms using ferumoxytol, a superparamagnetic iron oxide nanoparticle. J Cereb Blood Flow Metab. 2013; 33:780–786. [PubMed: 23486297]

35. Nalder S, Hidalgo J, Bloch T. Prediction of blood volume in normal human adults. Surgery. 1962; 51:542–551.

36. Berry LR, Barck KH, Go MA, et al. Quantification of viable tumor microvascular characteristics by multispectral analysis. Magn Reson Med. 2008; 60:64–72. [PubMed: 18421695]

37. Carano RA, Ross AL, Ross J, Williams SP, Koeppen H, Schwall RH, Van Bruggen N. Quantification of tumor tissue populations by multispectral analysis. Magn Reson Med. 2004; 51:542–551. [PubMed: 15004796]

38. R: a language and environment for statistical computing. R Foundation for Statistical Computing. 2013. http://www.R.project.org

39. Marcus CD, Ladam-Marcus V, Cucu C, Bouche O, Lucas L, Hoeffel C. Imaging techniques to evaluate the response to treatment in oncology: current standards and perspectives. Crit Rev Oncol Hematol. 2009; 72:217–238. [PubMed: 18760935]

40. Zhu H, Melder RJ, Baxter LT, Jain RK. Physiologically based kinetic model of effector cell biodistribution in mammals: implications for adoptive immunotherapy. Cancer Res. 1996; 56:3771–3781. [PubMed: 8706023]

41. Bremer C, Mustafa M, Bogdanov A Jr, Ntziachristos V, Petrovsky A, Weissleder R. Steady-state blood volume measurements in experimental tumors with different angiogenic burdens a study in mice. Radiology. 2003; 226:214–220. [PubMed: 12511693]

42. Persigehl T, Wall A, Kellert J, Ring J, Remmele S, Heindel W, Dahnke H, Bremer C. Tumor blood volume determination by using susceptibility-corrected DeltaR2* multiecho MR. Radiology. 2010; 255:781–789. [PubMed: 20501715]

43. Daldrup-Link HE, Golovko D, Ruffell B, et al. MRI of tumor-associated macrophages with clinically applicable iron oxide nanoparticles. Clin Cancer Res. 2011; 17:5695–5704. [PubMed: 21791632]

44. Tropres I, Lamalle L, Peoc'h M, Farion R, Usson Y, Decorps M, Remy C. In vivo assessment of tumoral angiogenesis. Magn Reson Med. 2004; 51:533–541. [PubMed: 15004795]

Author Manuscript

Author Manuscript

Author Manuscript

Author Manuscript
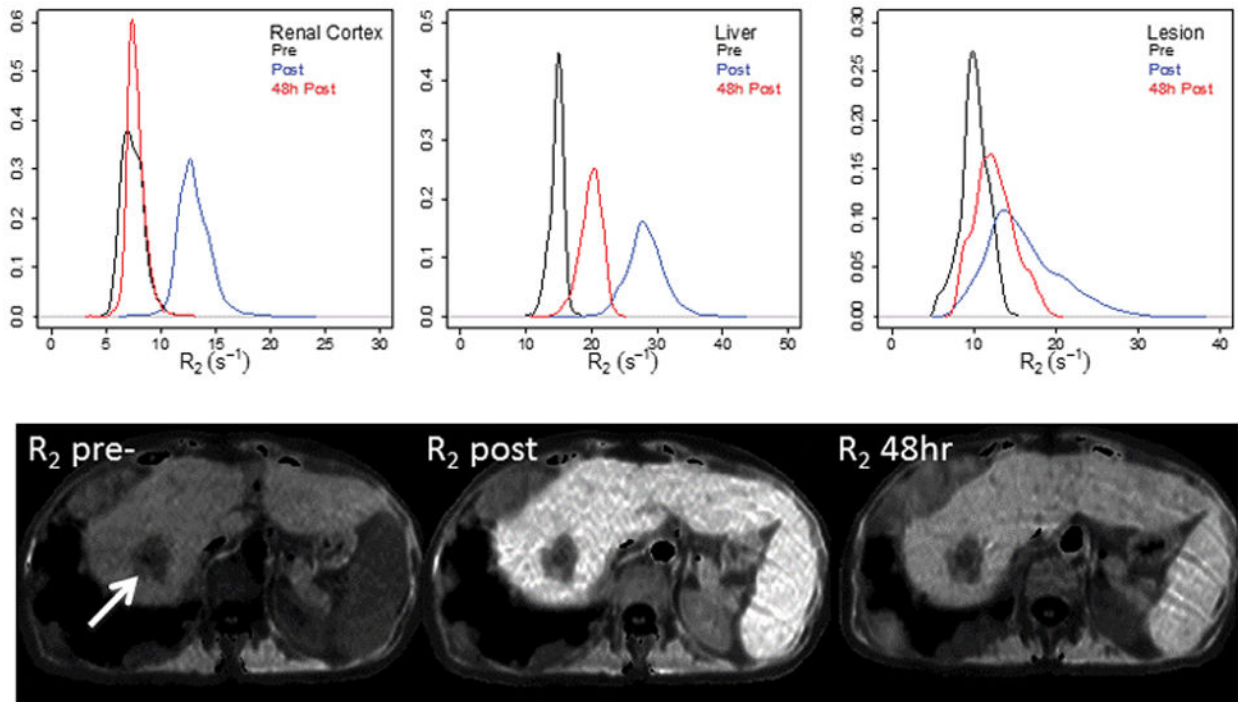
Figure 1.
Histograms and images of transverse relaxation rate (R_2), pre- and post-ferumoxytol injection in renal cortex (a), liver (b), and liver lesion (c) in a representative patient with liver and lung metastases from colorectal cancer. The primary target lesion is indicated by the arrow.
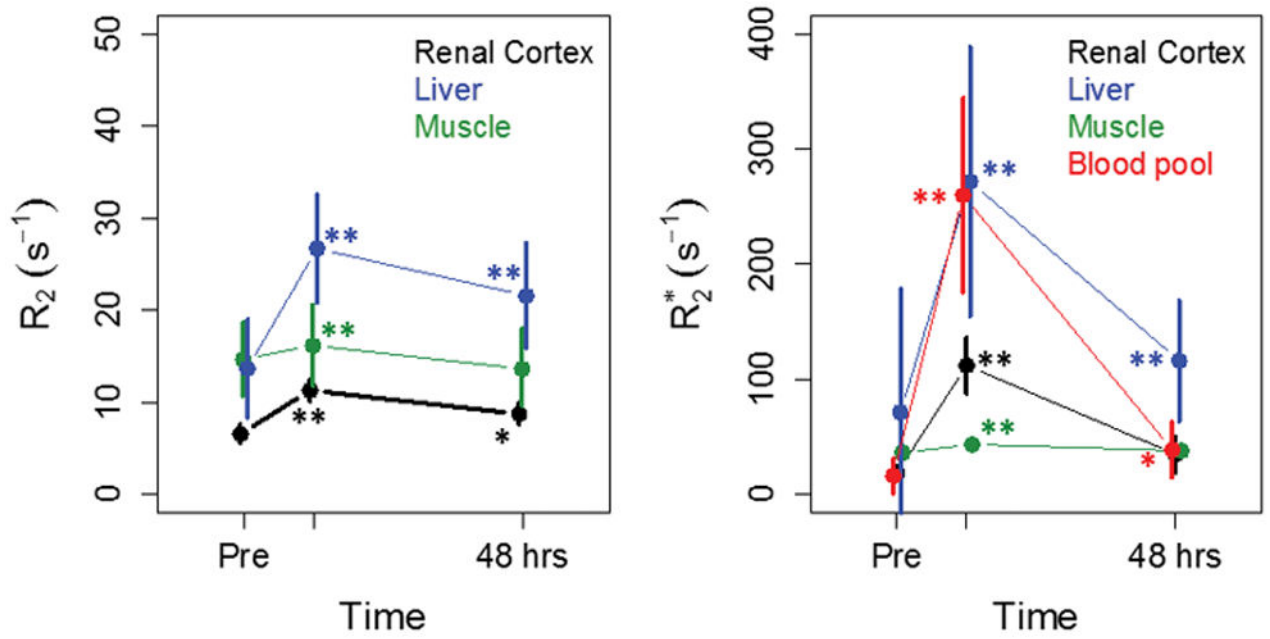
Figure 2.
Mean (±SD) of R_2 (a) and R_2^* (b) in normal tissues as a function of time for all patients. Significant changes in R_2 and R_2^* compared to pre- values are indicated by ** ($p<0.005$) and * ($p<0.05$), assessed by paired t-test. Similar patterns of change were seen on Day 15 scans.
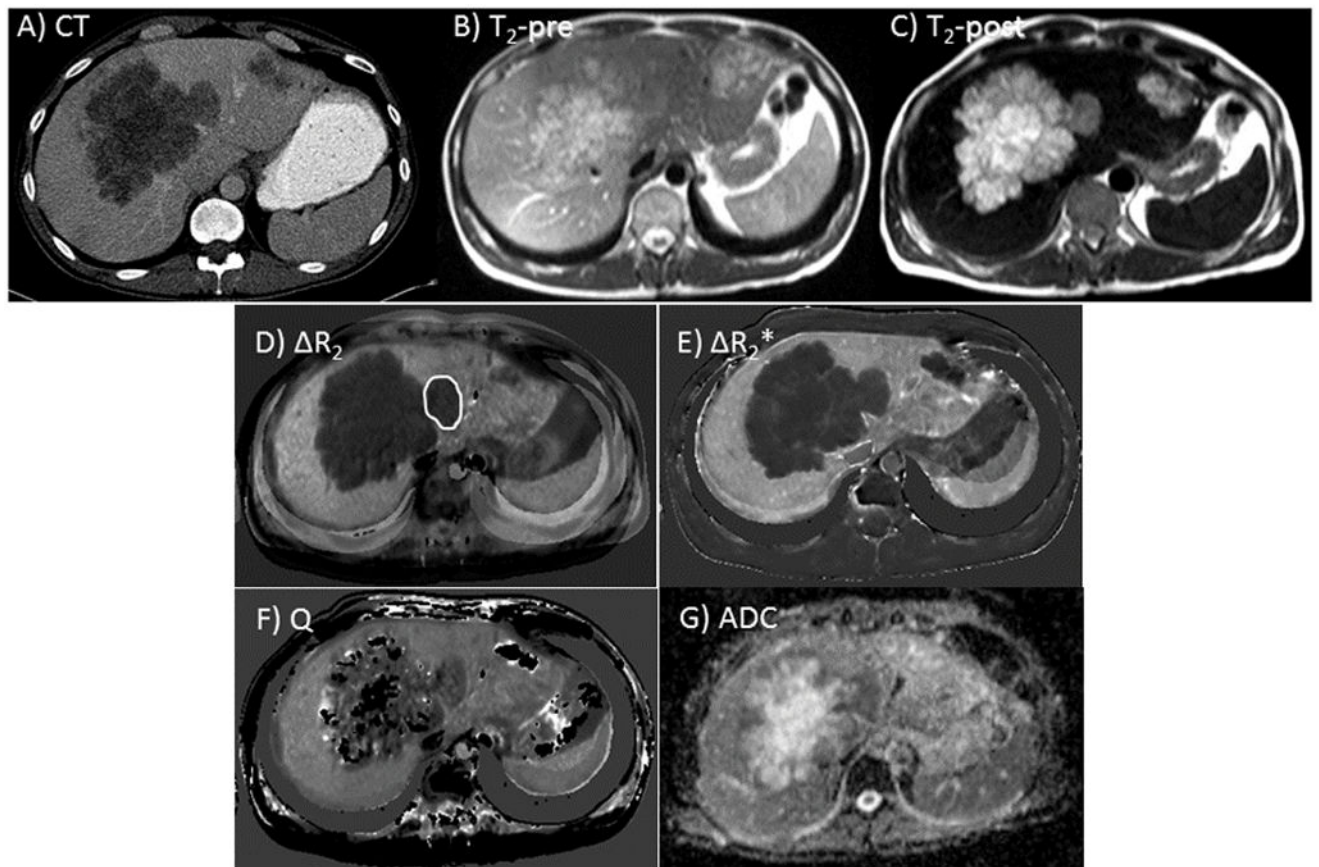
Figure 3.
Diagnostic CT (a), pre- (b) and post-ferumoxytol (c) T_2-weighted MRI scans from a representative patient with several large, partially necrotic liver metastases from colorectal cancer. R_2 and R_2* maps (d, e) and Q and ADC maps (f, g) are also shown. The target lesion for ROI measurements is highlighted in (d).

	CV (%)
ΔR_2	13.7
$\Delta R_2{}^*$	12.3
Q	14.0
ADC	4.9
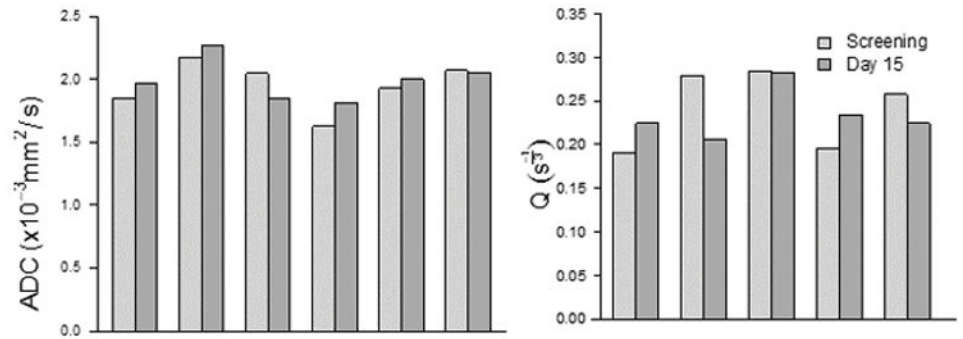
Figure 4.
Tabulation of coefficient of variation (%) calculated from screening and Day 15 measurements in the renal cortex, as an indication of repeatability of the measures. Repeated measures of ADC (a) and Q (b) in the renal cortex are relatively consistent across the group of subjects.
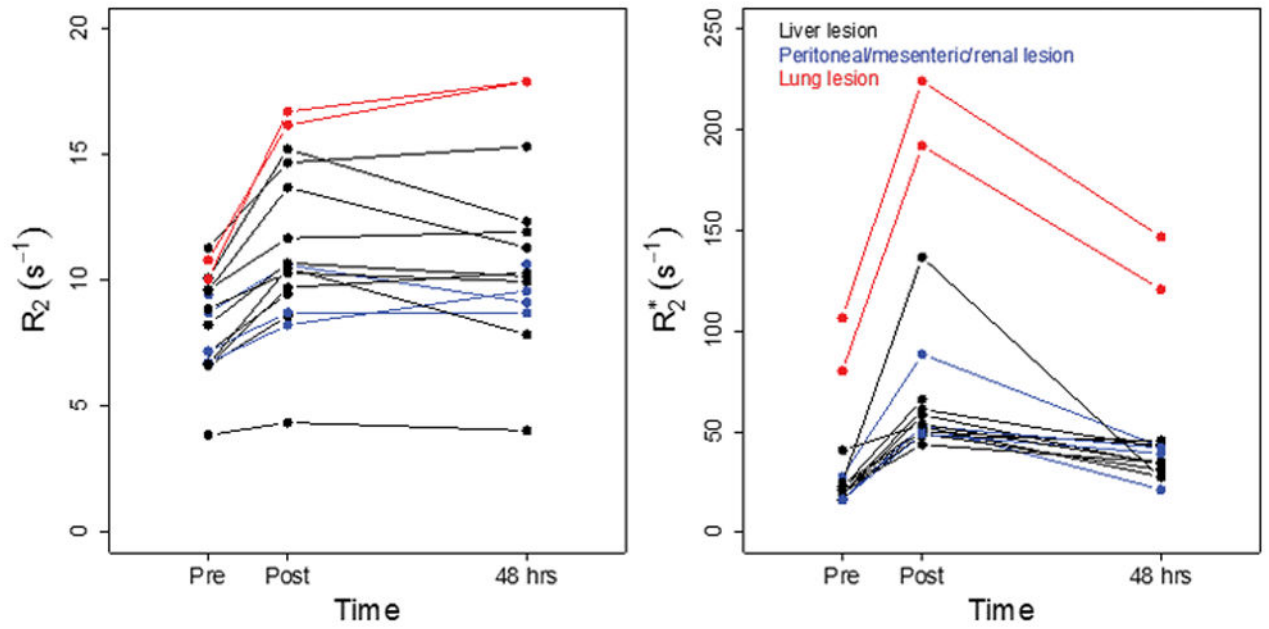
Figure 5.
Relaxation rate changes in target lesions. Mean of R_2 (a) and R_2^* (b) in individual lesions, color coded by location.
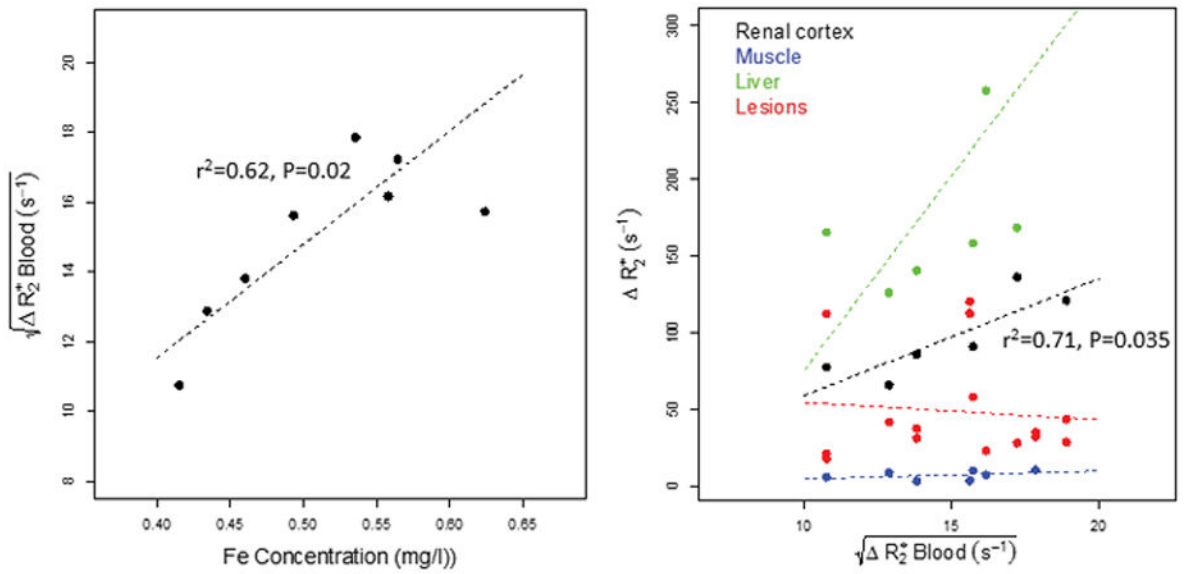
Figure 6.
Median R$_2$ (a), R$_2$* (b), Q (c), and ADC (d) for all lesions. The shaded bars represent mean ± SD measured in normal renal cortex (n=7).
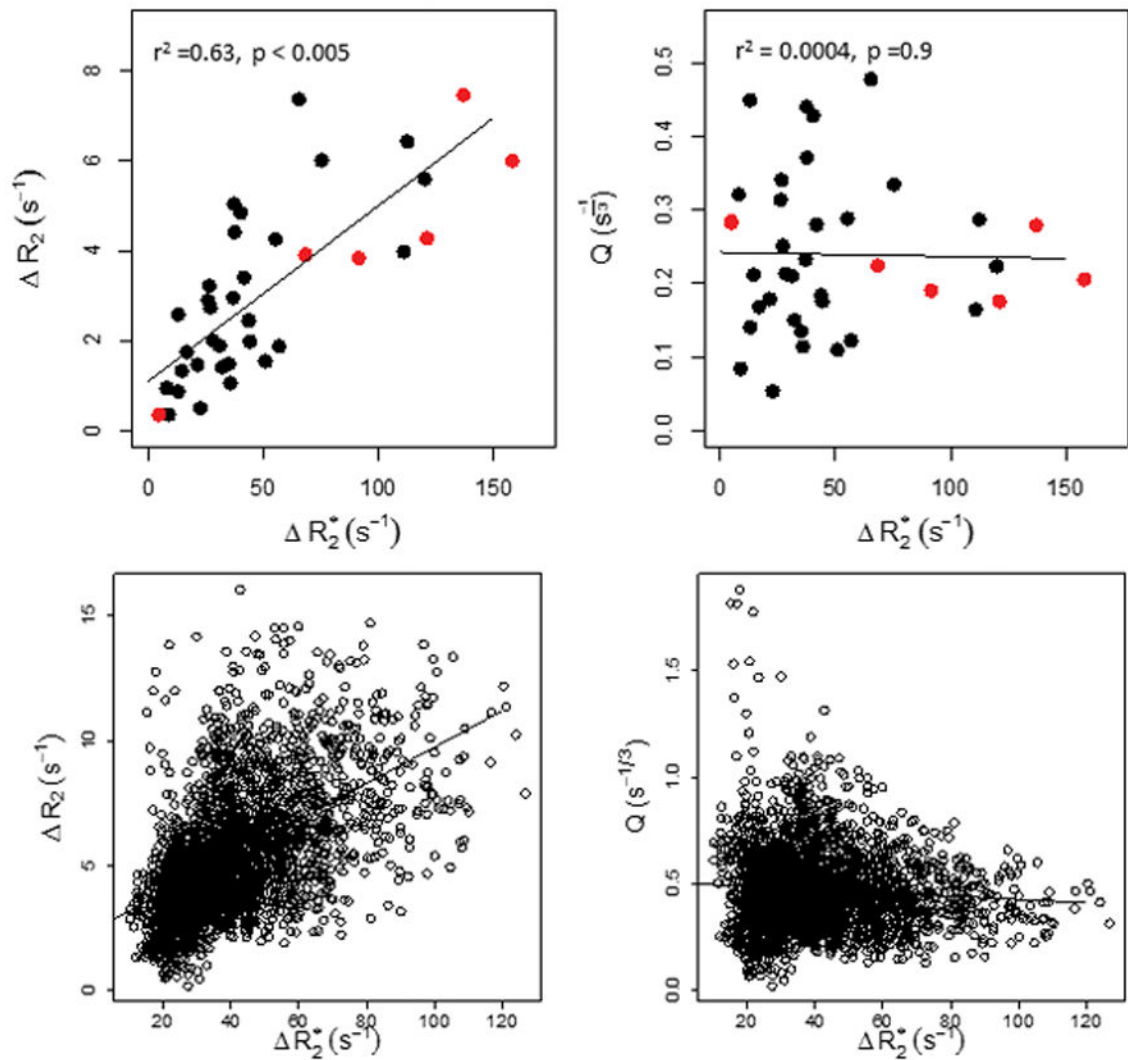
Figure 7.
(a) Linear relationship between estimated contrast agent (Fe) concentration in blood and the square root of R$_2$* in blood; points represent data from individual subjects. (b) Relationships between R$_2$* in tumor, renal cortex, liver, and muscle vs. the square root of R$_2$* in blood as a surrogate for blood iron concentration. Relative tissue slopes are consistent with results published by Bjornerud et al.
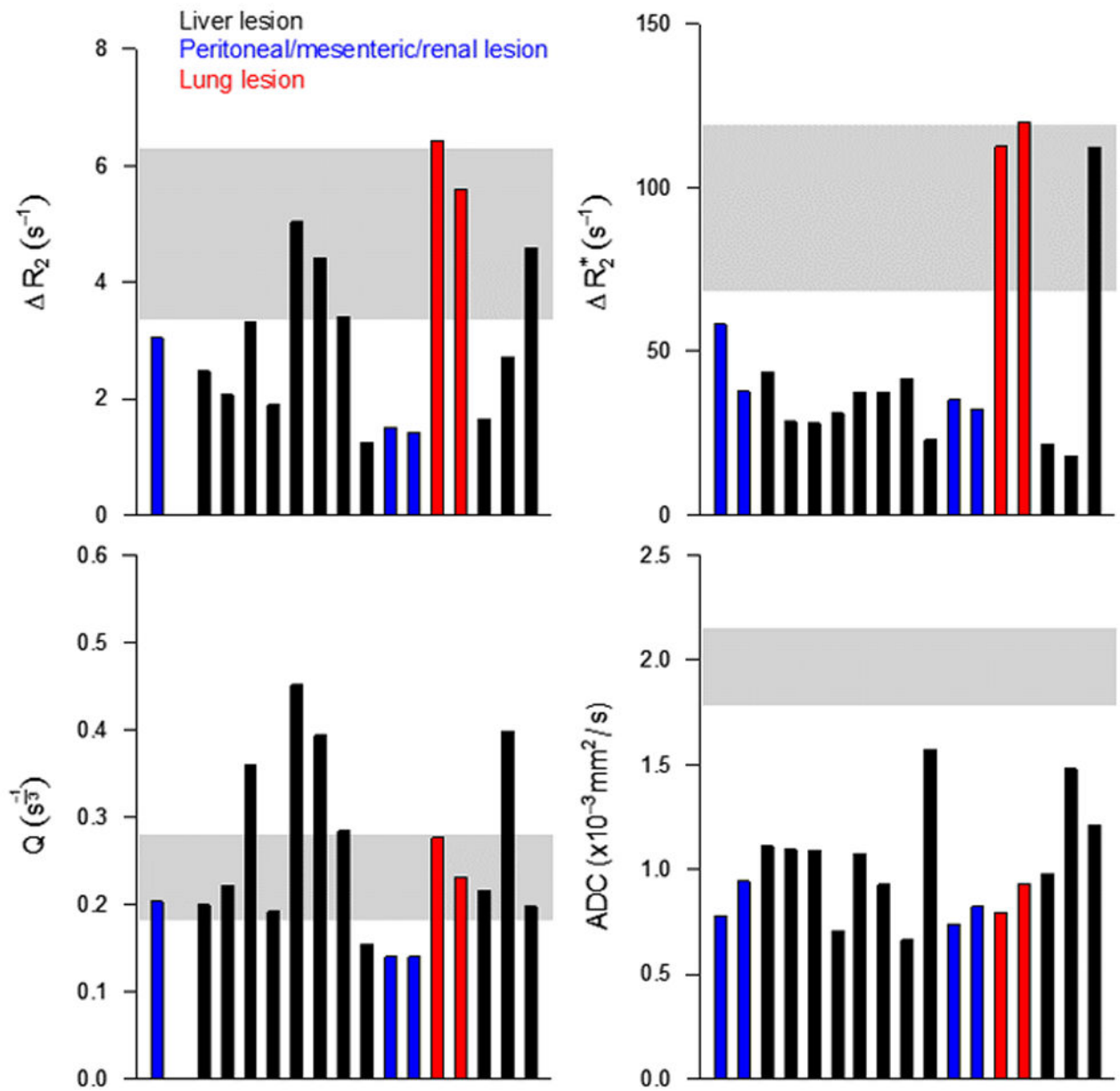
Figure 8.
ΔR₂ and Q as a function of tissue ΔR₂* for average lesion (red) and renal cortex (black) measurements (a,b), and for all voxels within one representative target lesion (c,d). As predicted by Jensen et al., Q is relatively insensitive to ΔR₂*.
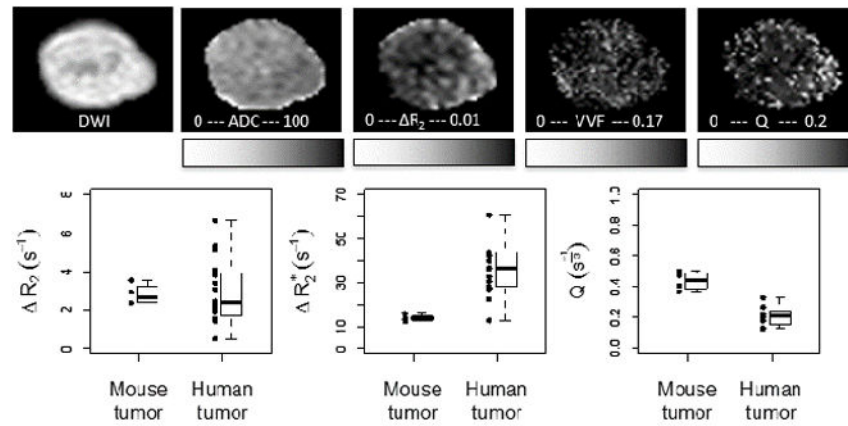
Figure 9.
Representative diffusion-weighted image and maps of ADC, R_2, R_2*, and Q of an HM-7 xenograft tumor grown on the hindlimb of an athymic nude mouse. Range of R_2, R_2* and Q (a, b, c) measured in HM-7 xenograft tumors in mice as well as all evaluated tumors in humans. Points represent individual results, while boxplots summarize the group data.